

## Acoustic vibrations of semiconductor nanocrystals in doped glasses

Prabhat Verma, W. Cordts, G. Irmer, and J. Monecke

*Institute of Theoretical Physics, Freiberg University of Mining and Technology, Bernhard-von-Cotta-Strasse 4, 09596 Freiberg, Germany*

(Received 23 February 1999)

Polarization-dependent low-frequency off-resonant Raman scattering has been studied from various commercially available filter glass samples, which contain  $\text{CdS}_x\text{Se}_{1-x}$  nanoparticles embedded in a glass matrix. In order to distinguish the confined acoustic phonons from the glass background, the spectra have been compared with those obtained from the base material, which does not contain nanoparticles. Polarized and depolarized scattering from confined acoustic phonons was distinctly resolved near the laser line and overtones of the polarized modes were observed. A theoretical treatment, which establishes a relation between the particle size, the frequencies, and the widths of various phonons, taking into account the matrix influence on the vibrational spectrum and on its damping, is presented. The material-dependent generalized form of this model enables one to use it for any given combination of particle and matrix materials. A good agreement between the experimental and the theoretical results is found. The nanoparticle sizes obtained from Raman scattering agree well with those obtained from transmission electron microscope and anomalous small angle x-ray scattering experiments. [S0163-1829(99)07231-8]

### I. INTRODUCTION

In recent times, the optical properties of quantum confined electronic systems such as quantum wells, quantum wires, and quantum dots have attracted considerable attention, because they differ strongly from those of the corresponding bulk crystal. Especially, the electronic and optical properties of semiconductor nanocrystals embedded in solid matrices such as CuCl in NaCl (Refs. 1 and 2) and CuCl, CdS, CdSe,  $\text{CdS}_x\text{Se}_{1-x}$ , and Ge in glass<sup>3-13</sup> have been studied in the past decade. Specific attention has been paid<sup>8-13</sup> to silicate glasses in which CdS or  $\text{CdS}_x\text{Se}_{1-x}$  nanoparticles are grown by special thermal treatment. These glasses are the basis for commercially available sets of yellow to red sharp cut filters, which are very attractive from a fundamental point of view as well as for their potential use in the field of the nonlinear optics, where it is critical to have an accurate knowledge of the size distribution of the particles. In a small nanocrystal with size in the range of a few nanometers to a few tens of nanometers, spatial confinement effects on the electron-hole system and on the propagation of phonon become significant. Due to this confinement, nanoparticles exhibit distinct physical properties which have been studied in the recent past<sup>8-19</sup> both experimentally and theoretically. However, at present the information on the fundamental physical properties of such a system is insufficient, and much more information and knowledge is required in order to use them as optical processing devices. A deeper knowledge of the vibrational properties is necessary and it is indispensable to consider the confinement effects on the vibrational properties of such a system.

Raman scattering, which is sufficiently influenced by surface conditions, particle sizes, and size distribution of a nanoparticle system, is one of the most important and non-destructive techniques to obtain information about the vibrational and electronic states in a confined system. In previous studies,<sup>9-19</sup> special attention has been paid to the low-frequency Raman scattering from elastic spherical nanoparticles, which vibrate with frequencies inversely proportional

to their diameter. A peak in the low-frequency range was observed in Raman scattering from symmetric and quadrupolar acoustic vibrations of these spherical particles, and the particle size was deduced from the energy of this peak. Following the treatment of Lamb<sup>20</sup> from the end of the 1800s, these vibrations are usually described as the eigenfrequencies of a homogeneous elastic sphere under stress-free boundary conditions, and are classified into two categories, torsional and spheroidal, the torsional modes being Raman inactive. These modes can be classified according to the symmetry group of the sphere by the angular quantum number  $l$  ( $=0,1,2,\dots$ ), which measures the number of wavelengths along a circle on the surface of the particle. The  $l=0$  spheroidal modes are purely radial with spherical symmetry, and at higher values of  $l$  an angular corrugation appears. Another index  $p$  ( $=1,2,3,\dots$ ) distinguishes the lowest-order mode ( $p=1$ ) from its overtones ( $p\geq 2$ ) in the Raman spectra. Duval<sup>21</sup> has shown that the spheroidal modes with  $l=0$  and  $l=2$  are the only Raman active modes. However, the  $l=1$  mode also becomes Raman active under resonant conditions.<sup>22</sup> The  $l=0$  mode is completely polarized and the  $l=2$  mode is depolarized for a perfect sphere. After Duval, this problem has been studied by some other authors<sup>8-13</sup> for semiconducting nanoparticles embedded in glass. In most cases,<sup>8,11-13</sup> only one structure in the low-frequency range was observed and no specific polarization properties were reported, however. Tanaka, Onari, and Arai<sup>10</sup> have discussed polarization properties, but for most of their samples they could observe only one structure, which they identified as a combination of polarized ( $l=0, p=1$ ) and depolarized ( $l=2, p=1$ ) modes. They could observe a trace of the depolarized ( $l=2, p=1$ ) mode in the cross-geometry configuration only for the smallest particle in the form of a shoulder on the Rayleigh background. Overtones of the confined phonons ( $p>1$ ) were not reported in the past.

The frequency positions of elastic vibrations are inversely proportional to the particle size<sup>9</sup> and, therefore, they are very close to the laser line for samples with larger particles. A set of very careful experiments is needed to observe and to re-

solve distinctly the polarized and depolarized modes. In this paper, we present a systematic study of the low-frequency Raman scattering from  $\text{CdS}_x\text{Se}_{1-x}$  nanocrystals embedded in a glass matrix. In our experiments, we have been able to measure Raman spectra down to about  $3 \text{ cm}^{-1}$  in both the Stokes and the anti-Stokes spectral ranges from a set of samples. We have observed both polarized and depolarized phonon modes for all samples and have been able to resolve them distinctly in polarization-dependent experiments. Further, we have observed some of the overtones of the polarized mode. These observations, to the best of our knowledge, have been reported here for the first time. The overtones of the depolarized modes overlap with the lower-order polarized modes, which prevents us from observing them in our experiments. Further, a theoretical description is presented to discuss the vibrational spectra of a spherical nanoparticle embedded in a matrix, taking into account appropriate boundary conditions. The resulting complex nature of the eigenvalues due to radiation decay enables us to estimate both vibrational frequencies and their dampings. This generalized calculation, compared to previously reported work,<sup>10,20,23</sup> can be used to estimate the vibrational spectra along with damping for any given set of materials. We have estimated the average size of the nanoparticles for various samples from our theoretical considerations using the experimental values of the vibrational frequencies of the first-order polarized mode. Using these results, the vibrational frequencies of the overtones and of the depolarized mode, and the phonon width of all vibrations are calculated and are found in good agreement with the corresponding experimental values. The composition  $x$  in the mixed  $\text{CdS}_x\text{Se}_{1-x}$  crystal, which is needed in the calculation, was estimated from optical phonons in near-resonant Raman scattering experiments. In order to have an independent estimate, the results obtained from Raman scattering were compared with those obtained from transmission electron microscope (TEM) and anomalous small angle x-ray scattering (ASAXS) measurements in an independent study.<sup>24</sup>

## II. EXPERIMENTAL DETAILS

The samples investigated are orange and red sharp-cut filter glasses procured from Schott Glass Inc., Germany. The commercial names of the samples are OG515, OG530, OG550, OG590, RG630, RG645, RG665, and RG695, where the numbers indicate the cutoff wavelengths in nanometers, and OG and RG stand for orange and red glasses, respectively. These filters contain  $\text{CdS}_x\text{Se}_{1-x}$  nanocrystallites of dimensions of the order of nanometers, embedded in a borosilicate glass matrix. The cutoff wavelength for various glasses depends both on the composition  $x$  and the particle size. A sharp cutoff in the band edge was observed both in absorption spectra and in photoluminescence measurements.<sup>25</sup>

Low-frequency Raman scattering experiments were performed at room temperature using an argon-ion-laser-pumped Ti-sapphire laser, a triple-stage Jobin Yvon monochromator, a liquid-nitrogen cooled CCD detector, and usual electronics. In order to avoid a strong luminescence background, the samples were excited well below the band gap with a probing wavelength of 836 nm. The optical phonons

were measured in near-resonance condition with the 488 nm line of an Ar-ion laser. The heat conduction from the isolated nanoparticles to the surrounding matrix is low and, hence, the sample temperature can increase considerably<sup>25</sup> due to the local heat produced by the probing laser. Therefore, experiments were performed at low laser power in a perpendicular scattering geometry, so that no changes in the optical properties due to laser heating could be observed. Raman measurements were performed in both parallel and perpendicular polarization geometries.

In order to estimate the particle size, shape, and size distribution in an independent way, the samples were characterized using TEM and ASAXS measurements. It was observed from the TEM photographs that the particle shapes deviate only slightly from perfect spherical ones and do not show large fluctuation of the particle size within a sample. From the results obtained in ASAXS measurements, size distribution within each sample could be best fitted with a distribution width of about 1 nm, which varies slightly from sample to sample.<sup>24</sup> The volume fraction of nanoparticles was estimated to be about 0.2% in both TEM and ASAXS measurements.

## III. THEORETICAL CONSIDERATIONS

An acoustic phonon of large wavelength propagating through a bulk crystal can be described by the classical theory of vibrations of a continuous elastic body. In the case of a confined acoustic phonon within the small volume of a nanoparticle, appropriate boundary conditions on the surface of the particle have to be taken into account. Supported by Lamb's results<sup>20</sup> for the free vibrations of a homogeneous spherical elastic body, the theory was extended by many authors<sup>8-11,19,26</sup> for the case of the confined acoustic phonon in nanoparticles with special emphasis on the matrix influence, on surface relaxation, and on shape anisotropy effects. Such calculations start with the equation of motion for a spherical elastic body under stress-free boundary conditions, which can be solved by introducing proper scalar and vector potentials, and then the energy spectrum for confined vibrations is obtained. These vibrations are classified into spheroidal and torsional modes with angular quantum number  $l$ , with only  $l=0$  and  $l=2$  modes being Raman active.<sup>21</sup> For particles embedded in a matrix, the basic relation for the continuity of the displacement and of the stress vectors at a spherical surface (see the Appendix) results in a generalized eigenvalue equation, which was discussed earlier for a free particle in Ref. 20 and for an embedded particle in Ref. 23. For the polarized vibrations ( $l=0$ ) of a spherical isotropic elastic particle with free boundary conditions, it is given as<sup>23</sup>

$$\sin(\xi) = 4n^2 j_1(\xi), \quad (1)$$

where  $j_1(\xi)$  is the spherical Bessel function of the first kind of order 1, with the dimensionless argument

$$\xi = R \frac{\omega}{v_l}, \quad (2)$$

where  $R$  is the particle radius and  $\omega$  is the vibrational frequency. The parameter  $n$ , an internal acoustic index, is the ratio of the transverse and longitudinal sound velocities

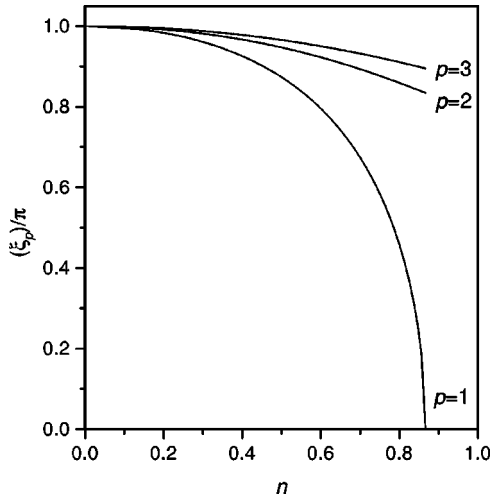


FIG. 1. The  $n$  dependence of the first three eigenvalues in Eq. (3). In order to compare the relative behavior of the three modes, the curves for  $p=2$  and  $p=3$  are shifted by  $-1$  and  $-2$ , respectively.

$v_t/v_l$  in the particle. Since the transverse sound velocity in a liquid is zero, the index  $n$  gives a measure for the deviation from the vibrational behavior of a liquid drop and its dimensionless spectrum  $\xi_p^{(0)} = p\pi$  with non-negative integers  $p$ .

Equation (1) can be solved by iteration,

$$\sin(\xi_p^{n+1}) = 4n^2 j_1(\xi_p^n). \quad (3)$$

Starting with the spectrum of a liquid drop, the iteration procedure converges quite fast and for  $p \geq 3$ , the first approximation

$$\xi_p^{(1)} = p\pi - \arcsin\left(\frac{4n^2}{p\pi}\right), \quad (4)$$

gives a reasonably good solution. The dependence of the first three eigenvalues on the index  $n$  is calculated numerically and shown in Fig. 1. Though the index  $n$  is limited to  $\sqrt{2}/2$ , the curves in Fig. 1 are shown up to  $n = \sqrt{3}/2$ , because the frequency of the first mode ( $p=1$ ) vanishes at this point. For all other eigenvalues ( $p \geq 2$ ) the asymptotic limit is given by the zeros of the spherical Bessel function  $j_1(\xi)$  representing the spectrum of a sphere with the radius fixed at  $R$  with zero displacement.

Next, we discuss the influence of a surrounding matrix on the polarized vibrational spectrum of a spherical particle. The eigenvalue equation in this case is similar to Eq. (1), with the only difference that the index  $n$  must be replaced by an effective complex value  $n_{\text{eff}}$  given as (see the Appendix)

$$n_{\text{eff}}^2 = n_s^2 - f \left[ n_m^2 - \frac{1}{4} \frac{(\kappa\xi)^2}{1 - i(\kappa\xi)} \right], \quad (5)$$

where  $n_s = v_{st}/v_{sl}$  and  $n_m = v_{mt}/v_{ml}$  are the ratios of the transverse to the longitudinal sound velocities in the sphere and in the matrix, respectively,  $\kappa = v_{sl}/v_{ml}$ , and  $f = \rho_m v_{ml}^2 / \rho_s v_{sl}^2$ , with  $\rho_m$  and  $\rho_s$  being the mass densities of the matrix and the sphere, respectively.  $n_{\text{eff}}$  being complex, the solutions of the eigenvalue equation are complex, too, the real and imaginary parts of which give the vibrational ener-

gies and their dampings due to sound radiation into the surrounding matrix, respectively. With  $f=0$ , one recovers the case of a free particle. Therefore,  $f$  can be considered as the coupling constant between the particle and the matrix. This coupling constant, determined essentially from the compression moduli ratio of the two materials, gives a measure for the influence of the matrix on the vibrational spectrum of the nanoparticle.

Replacing  $n$  by  $n_{\text{eff}}$  in Eq. (1), one finds a significant difference compared to the case of a free sphere in the asymptotic behavior for large values of the argument  $\xi$ . The right-hand side of the eigenvalue equation no longer vanishes but oscillates with the term  $-if\kappa \cos(\xi)$ . This results in a constant imaginary shift of the large eigenvalues by  $i/4 \ln(R_k)$ , where

$$R_k = \left( \frac{Z_m - Z_s}{Z_m + Z_s} \right)^2 \quad (6)$$

is the sound reflection coefficient of longitudinal waves at normal incidence, and  $Z_m = \rho_m v_{ml}$  and  $Z_s = \rho_s v_{sl}$  are sound impedances of the matrix and of the sphere, respectively. We would like to mention here that these asymptotic imaginary parts of the vibrational spectra give upper limits to the damping.

If the matrix impedance is larger than the sphere impedance ( $f\kappa = Z_m/Z_s > 1$ ), the large eigenvalues  $\xi_p$  undergo an additional shift by a real amount of  $\pi/2$ . For large  $p$ , the asymptotic spectra become

$$\xi_p \approx p\pi + \frac{i}{4} \ln(R_k), \quad (7)$$

for a hard sphere in a soft matrix, and

$$\xi_p \approx \frac{2p+1}{2} \pi + \frac{i}{4} \ln(R_k), \quad (8)$$

for a soft sphere in a hard matrix.

The lower-order eigenvalues, which are of greater interest in our case, deviate only slightly from the asymptotic spectra. Thus one can calculate them again by iteration starting from the asymptotic values of Eqs. (7) and (8).

The qualitative behavior of the first eigenvalues, however, can be deduced directly from the effective index  $n_{\text{eff}}$ . Since the eigenvalues  $\xi_p$  lie near the real axis, the real part of  $n_{\text{eff}}^2$  is approximately equal to  $n_s^2 - f(n_m^2 - 1/4)$ . As a result, the real parts of the eigenvalues are shifted with respect to Fig. 1 to higher values in a hard matrix with  $n_m^2 > 1/4$  and to lower values in a soft matrix. It is interesting to mention that the matrix properties are alone responsible for the direction of the frequency shift and the relative properties of the sphere and the matrix have no influence.

After calculating the eigenvalue  $\xi$ , a relation between  $\omega$  and  $R$  can be established from Eq. (2). Since  $\xi$  is of complex nature,  $\omega$  can be expressed as

$$\omega = \omega' + i\Delta\omega' = \frac{v_l}{R} \xi, \quad (9)$$

where the real and the imaginary parts give the phonon frequencies and half-widths, respectively. It is interesting to

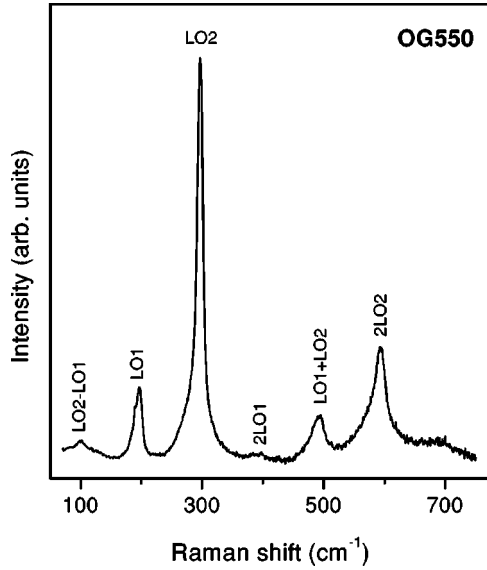


FIG. 2. Near-resonant Raman spectrum for the sample OG550, showing the optical phonons and their combinations.

mention that the phonon widths also show the same dependence on the particle size ( $\propto 1/R$ ) as the phonon frequencies.<sup>9</sup> Therefore, the phonon lines are sharper for larger nanoparticles.

Unfortunately, an effective procedure for the depolarized mode with  $l=2$ , similar to that discussed for the  $l=0$  mode, cannot be obtained. The eigenvalue equation, in this case, contains functions with two different periodicities, due to the two sound velocities  $v_l$  and  $v_l$ . The eigenvalue spectrum is very sensitive to the material parameters, and cannot be obtained analytically. However, the qualitative behavior of the spectrum is, in general, similar to that of the polarized mode with  $l=0$ . The matrix influence shifts the frequency positions in the same direction and phonon frequencies and widths also show the same dependence on the particle size, i.e., they are proportional to  $1/R$ . The theoretical values for the  $l=2$  mode were calculated numerically with the help of the general eigenvalue equation given in the Appendix [Eq. (A20)]. We will show in the next section that this gives a good quantitative agreement with the experimental measurements of the depolarized phonon modes.

## IV. RESULTS AND DISCUSSION

### A. Optical phonons

In order to estimate the sound velocity in the nanoparticles, we estimated the composition  $x$  from the positions of the optical phonons in the near-resonance Raman spectra of various samples. A mixed  $\text{CdS}_x\text{Se}_{1-x}$  crystal shows a two-mode behavior with two LO phonons, one corresponding to CdSe and the other corresponding to CdS. The near-resonance Raman spectra of one of the samples in the optical range is presented in Fig. 2, where LO1 represents the CdSe-like and LO2 the CdS-like mode. In addition, some higher-order phonons are also seen. The LO phonons in these samples are shifted in energy with respect to the LO phonons in pure CdSe and CdS bulk materials due to the mixed crystal behavior and due to the spatial confinement in small particles. The shift due to confinement originates from the relaxation of the  $\mathbf{q}$  vector selection rule,<sup>27</sup> as the spatial correlation function becomes finite. However, this shift is small<sup>27</sup> ( $2 \text{ cm}^{-1}$  or less) for nanoparticles of diameter above 5 nm. We roughly assumed a shift due to confinement of  $1 \text{ cm}^{-1}$  for all samples. This assumption is reasonable because the variation in this shift from one sample to the other is much smaller compared to the shift due to the change of composition, which was found to be as large as  $20 \text{ cm}^{-1}$  for some samples compared to pure CdSe and CdS bulk material. Assuming a linear shift in the LO-phonon energies with respect to the composition  $x$ , the value of  $x$  was calculated for each sample from the positions of both LO1 and LO2, and is listed in Table I. However, we will see later that the influence of the composition on the frequencies of the confined vibrations is weak.

### B. Confined acoustic phonons

Low-frequency Raman spectra from the sample OG550 are presented as an example in Fig. 3, where curves (a) and (b) correspond to polarized and depolarized configurations, respectively. For comparison, an unpolarized Raman spectrum from the base material used for OG550 is presented as curve (c). The base material is the material before heat treatment, and, therefore, does not contain any semiconducting nanoparticles. This was also confirmed in luminescence<sup>25</sup>

TABLE I. Composition  $x$ , particle radius  $R$ , and experimental and theoretical values of the phonon frequencies in low-frequency Raman scattering for various filter glass samples.  $\omega_{21}$  and  $\omega_{22}$  are the depolarized phonon frequencies for the lowest  $l=2$  mode and its first-order overtone, respectively,  $\omega_{01}$ ,  $\omega_{02}$ , and  $\omega_{03}$  are the polarized phonon frequencies for the lowest  $l=0$  mode and its first and second overtones, respectively. The experimental values  $\omega_{01}$  have been used to determine  $R$ . All frequencies are given in  $\text{cm}^{-1}$ .

Sample	$x$	$R$ (nm)	$\omega_{21}$ Expt./Theor.	$\omega_{22}$ Expt./Theor.	$\omega_{01}$ Expt.	$\omega_{02}$ Expt./Theor.	$\omega_{03}$ Expt./Theor.
OG515	0.67	2.17	16.0/14.3	-/26.8	29.3	-/60.6	-/91.3
OG530	0.67	2.22	13.8/13.9	-/26.1	28.6	57.5/59.1	-/89.1
RG630	0.27	3.40	8.8/8.7	-/16.2	17.6	37.0/36.4	-/54.8
OG550	0.67	3.65	8.5/8.5	-/15.9	17.4	39.8/36.0	54.1/54.2
OG590	0.54	4.42	7.3/6.9	-/12.9	14.1	31.6/29.1	49.0/43.9
RG695	0.26	5.38	6.1/5.5	-/10.2	11.1	25.8/23.0	36.7/34.6
RG645	0.32	6.02	5.6/4.9	-/9.2	10.0	23.3/20.7	36.1/31.2
RG665	0.20	7.78	4.5/3.8	-/7.0	07.6	17.5/15.7	27.7/23.7

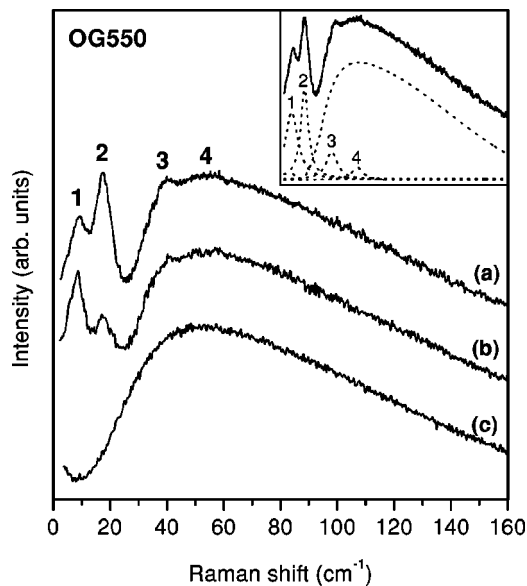


FIG. 3. Low-frequency Raman spectra for the sample OG550 in (a) polarized and (b) depolarized configurations. Curve (c) corresponds to the base material used for the sample. Inset presents a deconvolution of various modes seen in the spectra (a).

and ASAXS (Ref. 24) measurements. Curve (c) in Fig. 3 shows a broad structure at about  $50 \text{ cm}^{-1}$ , which is known as a Boson peak,<sup>28,29</sup> and is attributed to vibrations of the glass matrix. This structure is also present in curves (a) and (b). The spectra in Fig. 3 have been normalized to this broad structure for presentation. Apart from this structure, two distinct peaks, indicated by the indices 1 and 2, can be seen at  $8.5$  and  $17.5 \text{ cm}^{-1}$  in curves (a) and (b), which correspond to the confined acoustic vibrations of the  $\text{CdS}_x\text{Se}_{1-x}$  nanoparticles. Peak 1 in Fig. 3 is identified as the depolarized vibration with  $l=2$ ,  $p=1$  and peak 2 as the polarized  $l=0$ ,  $p=1$  vibration. Weak structures indicated by the indices 3 and 4 at  $40$  and  $54 \text{ cm}^{-1}$ , respectively, are identified as the first and the second overtones of peak 2 and correspond to the vibrations  $l=0$ ,  $p=2$ , and  $p=3$ , respectively. Besides the strong peak at  $8.5 \text{ cm}^{-1}$  ( $l=2$ ,  $p=1$ ) in the depolarized spectrum in curve (b), a second weak structure is seen at the calculated position of the first overtone of the depolarized mode ( $l=2$ ,  $p=2$ ). However, the position of this overtone overlaps with the position of peak 2 ( $l=0$ ,  $p=1$ ). Although the latter is forbidden in the depolarized configuration, it could have a slight component due to a possible slight deviation of our experimental configuration from the true depolarization geometry or due to the fact that the nanoparticles are not perfectly spherical, as indicated in TEM measurements. Therefore, it is difficult to assign this structure either to the  $l=2$ ,  $p=2$  mode or to the  $l=0$ ,  $p=1$  mode. The higher-order overtones of the depolarized modes are weak and hidden in the boson background.

Figure 4 shows similar spectra from the sample RG665. In order to focus attention on the confined phonons and their overtones, the spectra are presented in a small spectral range. The polarized and depolarized phonons of this sample are very close to each other at  $4.5$  and  $7.5 \text{ cm}^{-1}$ , respectively. The first and the second overtones of the polarized vibration, indicated by the indices 3 and 4 in Fig. 4, can be seen at  $17$  and  $27.5 \text{ cm}^{-1}$ , respectively. A trace of higher-order over-

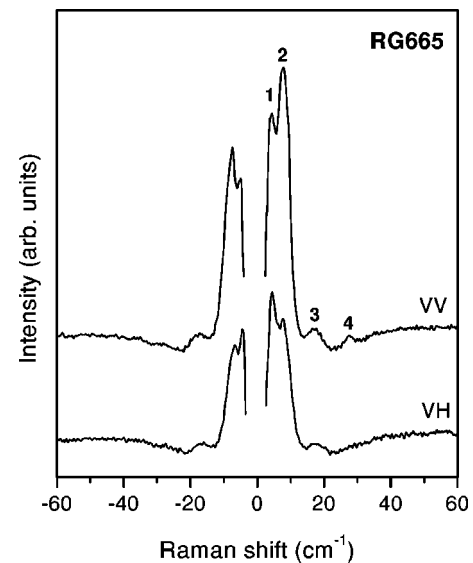


FIG. 4. Low-frequency Raman spectra in polarized and depolarized configurations for the sample RG665. Phonon modes indicated by 3 and 4 are the overtones of the phonon mode 2.

tones also appears, but they could not be resolved distinctly due to their weak oscillator strengths compared to the glass background in this spectral range. Similar results have been observed for other samples and they are presented in Figs. 5(a) and 5(b) in the polarized and depolarized configurations, respectively. These spectra are arranged in the order of increasing particle size and, thus, in decreasing phonon energy from the sample OG515 to the sample RG665. It can be seen from Fig. 5 that the scattering intensity increases and the separation between polarized and depolarized modes (peaks 1 and 2) decreases with increasing particle size. Peaks 1 and 2 are found to shift from  $4.5$  to  $16.0 \text{ cm}^{-1}$  and from  $7.5$  to  $29.5 \text{ cm}^{-1}$ , respectively, for various samples. In order to

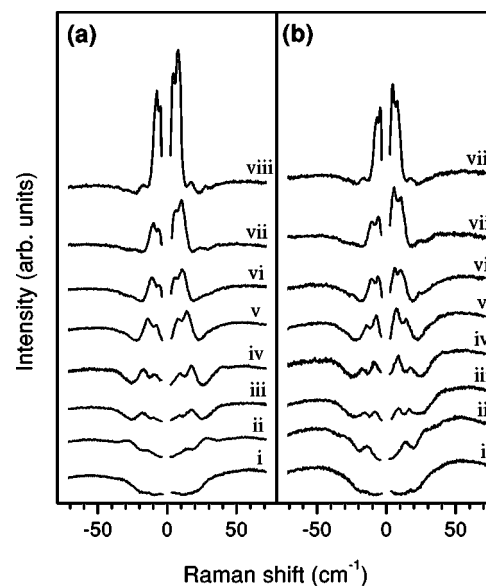


FIG. 5. Low-frequency Raman spectra in (a) the polarized and (b) the depolarized configurations for various samples. The spectra are arranged in a sequence of increasing particle size from curve (i) to curve (viii) for the samples OG515, OG530, RG630, OG550, OG590, RG695, RG645, and RG665.

TABLE II. Experimental and theoretical values of the phonon widths for some of the samples studied.  $\Gamma_{21}$  represents the phonon width for the depolarized first mode and  $\Gamma_{01}$ , represent the phonon widths for the polarized first mode and its first order overtone, respectively. All widths are given in  $\text{cm}^{-1}$ .

Sample	$R$ (nm)	$\Gamma_{21}$		$\Gamma_{01}$		$\Gamma_{02}$	
		Expt./Theor.	Expt./Theor.	Expt./Theor.	Expt./Theor.	Expt./Theor.	Expt./Theor.
OG530	2.22	7.5/9.9	9.7/13.1				
OG550	3.65	6.3/6.1	8.7/8.0			12.5/8.5	
OG590	4.42	6.5/4.8	8.2/6.3				
RG665	7.78	4.5/2.5	4.8/3.3			6.7/3.6	

obtain true values of the phonon widths and positions, a deconvolution was performed on each spectrum, an example of which is shown for OG550 in the inset of Fig. 3. This was done by assuming the phonons to have Lorentzian shapes and by choosing a suitable background, either from the spectra of the base material [as in Fig. 3(c)] when available, or from a combination of suitable mathematical functions. The measured values of phonon positions and widths for various samples are listed in Tables I and II, respectively.

The phonon corresponding to the lowest order polarized mode ( $l=0, p=1$ ) is the strongest phonon in Raman spectra. Using the experimental values of the phonon frequency of this mode, particle sizes were estimated from Eqs. (2) and (9), and from them the phonon frequencies and the widths for all polarized modes were calculated. The frequencies and the widths for the depolarized modes were numerically calculated from Eq. (A20) using the results obtained from the polarized modes. Table I lists the particle size and the phonon frequencies for various samples for all phonon modes. The phonon widths for various phonons in some of the samples are presented in Table II.

A good agreement between calculated and measured phonon frequencies is obtained (Table I). The measured values of phonon widths, as seen from Table II, are slightly larger than the calculated values. Only in the case of the sample OG530 are the measured values smaller than the calculated ones. However, it was not possible to measure the phonon widths for the sample OG515 within reasonable accuracy because the phonons have very weak strengths. The measured widths can be larger than the calculated ones due to two reasons: first, due to experimental errors coming from the equipment line function and, second, due to the size distribution of the nanoparticles within each sample. As mentioned earlier, the ASAXS measurements indicate a size distribution of about 1 nm for all samples. Due to this, the phonon energies are also distributed, which provides a broadening in the measured phonon widths. The difference between the measured and the calculated values is small and agrees well with a size distribution of about 1 nm. Further, the damping of the vibrations is calculated assuming the nanoparticles to have perfect spherical shape with a complete surface contact with the surrounding matrix. Both assumptions may not be valid if the particles are very small and, hence, the coupling constant  $f$  in Eq. (5) is effectively smaller. The actual phonon widths are then expected to be smaller than the calculated ones assuming a perfect spherical particle with complete surface contact. The smaller measured

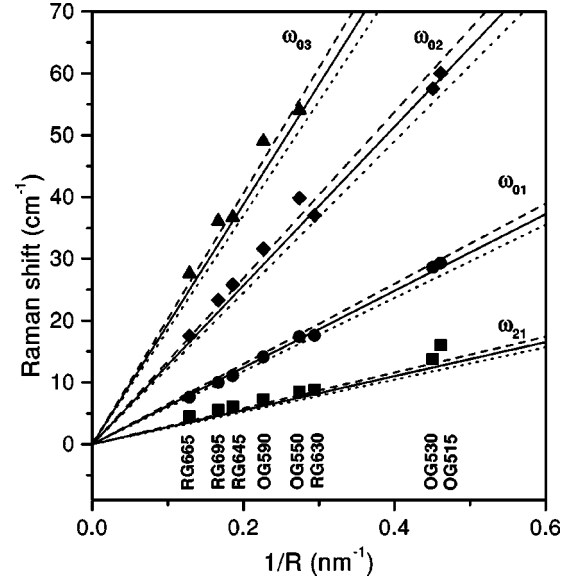


FIG. 6. Phonon positions with respect to  $1/R$  for various filter glass samples.  $\omega_{lp}$  represent various polarized modes, depolarized modes, and their overtones observed in low-frequency Raman spectra. The experimental values for the corresponding phonons are shown by full symbols. The dotted, full, and dashed lines correspond to the theoretical values calculated with  $x=0.8, 0.5,$  and  $0.2,$  respectively. It can be seen that the influence of the composition  $x$  on phonon frequencies is small.

values of the phonon widths for the sample OG530 in Table II can be explained in this way.

The theoretical results show that the influence of the composition  $x$  on the phonon frequencies is very small compared to the influence of the particle sizes. Figure 6 shows the relation between the phonon position and  $1/R$ . The three theoretical curves for each phonon are calculated for three different values of the composition  $x$  ( $=0.8, 0.5,$  and  $0.2$ ). It can be seen that the influence of the composition  $x$  is small, as stated before. The circles, the squares, and the triangles in Fig. 6 show the experimental phonon frequencies.

## V. CONCLUSIONS

Low-frequency Raman scattering has been performed on commercially available filter glass samples, which contain  $\text{CdS}_x\text{Se}_{1-x}$  nanoparticles embedded in a glass matrix. In our polarization-dependent experiments, we have been able to measure both polarized and depolarized confined acoustic phonons and to resolve them experimentally. Likewise, overtones of the polarized mode have been observed. A theoretical model, based on classical elasticity theory, which takes into account the influence of the matrix on the vibrational spectra of the nanoparticles, has been presented. This model establishes a relation between the particle size, the frequencies, and the widths of various confined phonons. It can be used for any given combination of particle and matrix materials. A good agreement between theoretical and experimental results has been found. In addition, the results obtained from Raman scattering are also found in good agreement with TEM and ASAXS measurements performed in an independent study.

## APPENDIX

The equation of motion of an elastic body

$$\frac{\partial^2 \vec{D}}{\partial t^2} = (v_l^2 - v_t^2) \nabla (\nabla \cdot \vec{D}) + v_t^2 \Delta \vec{D}, \quad (\text{A1})$$

for the displacement vector  $\vec{D}$  has the well known dilatation-free and curl-free solutions in spherical coordinates, which can be deduced from a scalar potential  $\Phi$  and a vector potential  $\vec{A} = \vec{r} \Psi$  as

$$\vec{D}_S = \nabla \Phi + \nabla \times \nabla \times \vec{A} = \vec{D}_1 + \vec{D}_2, \quad (\text{A2})$$

$$\vec{D}_T = k \nabla \times \vec{A}, \quad (\text{A3})$$

with

$$\Phi = \frac{1}{h} z_l(hr) Y_{lm}(\theta, \phi) \exp(-i\omega t), \quad (\text{A4})$$

$$\Psi = \frac{1}{k} z_l(kr) Y_{lm}(\theta, \phi) \exp(-i\omega t), \quad (\text{A5})$$

where  $Y_{lm}(\theta, \phi)$  are the spherical harmonics,  $z_l$  are the spherical Bessel functions,  $h = \omega/v_l$ , and  $k = \omega/v_t$ . The indices  $S$  and  $T$  in the displacement vector indicate the spheroidal and the torsional modes, respectively. It can be easily shown that the spheroidal displacement vectors have two independent directions, one along the radial unit vector  $\vec{e}_r$  and the other with a tangential component along  $\vec{n}_{lm}(\theta, \phi) = r \nabla Y_{lm}(\theta, \phi)$ . The torsional modes, however, have only one direction, namely, the orthogonal direction  $\vec{m}_{lm}(\theta, \phi) = \vec{e}_r \times \vec{n}_{lm}(\theta, \phi)$ . The same holds for the respective stress vectors also. Due to this, the spheroidal and torsional modes do not mix even due to the boundary conditions.

Since all displacement and stress vectors have a common time dependence, the factor  $\exp(-i\omega t)$  can be dropped in the following discussion. The displacement vectors  $\vec{D}_1$  and  $\vec{D}_2$  at the surface can be given, using the notation  $\vec{e}_{lm}(\theta, \phi) = Y_{lm}(\theta, \phi) \vec{e}_r$ , as

$$\vec{D}_1 = \nabla \Phi = D_{1r} \vec{e}_{lm} + D_{1n} \vec{n}_{lm}, \quad (\text{A6})$$

$$\vec{D}_2 = \nabla \times \nabla \times \vec{A} = D_{2r} \vec{e}_{lm} + D_{2n} \vec{n}_{lm}, \quad (\text{A7})$$

with

$$D_{1r}(hr) = z_l'(hr), \quad (\text{A8})$$

$$D_{1n}(hr) = \frac{z_l(hr)}{hr}, \quad (\text{A9})$$

$$D_{2r}(kr) = l(l+1) \frac{z_l(kr)}{kr}, \quad (\text{A10})$$

$$D_{2n}(kr) = \frac{z_l(kr)}{kr} + z_l'(kr). \quad (\text{A11})$$

The stress vectors  $\vec{S}_1$  and  $\vec{S}_2$  can be evaluated from the displacement vector as

$$\vec{S} = \rho \left( 2v_t^2 \frac{\partial \vec{D}}{\partial r} + v_t^2 \vec{e}_r \times (\nabla \times \vec{D}) + (v_l^2 - 2v_t^2) (\nabla \cdot \vec{D}) \vec{e}_r \right), \quad (\text{A12})$$

with

$$S_{1r}(hr) = h\rho [2v_t^2 D_{1r}'(hr) + (2v_t^2 - v_l^2) z_l(hr)], \quad (\text{A13})$$

$$S_{1n}(hr) = h\rho 2v_t^2 D_{1n}'(hr), \quad (\text{A14})$$

$$S_{2r}(kr) = k\rho 2v_t^2 D_{2r}'(kr), \quad (\text{A15})$$

$$S_{2n}(kr) = k\rho v_t^2 [D_{2n}'(kr) - z_l(kr)]. \quad (\text{A16})$$

For a free sphere, the independent stress vectors  $\vec{S}_1$  and  $\vec{S}_2$  have to be combined so that their superposition at the surface ( $r=R$ ) vanishes, and the eigenvalue equation becomes

$$\det \begin{pmatrix} S_{1r} & S_{2r} \\ S_{1n} & S_{2n} \end{pmatrix} \Big|_{r=R} = 0. \quad (\text{A17})$$

This equation can be rewritten into the form discussed by Tamura *et al.*<sup>23</sup> and by Tanaka *et al.*<sup>10</sup> For the special case of  $l=0$ , the dilatation-free displacement  $\vec{D}_2$  does not exist and  $\vec{D}_1$  has only the radial component. Therefore, the only remaining stress component is  $S_{1r}$ , and the eigenvalue equation reduces to

$$S_{1r}|_{r=R} = 0. \quad (\text{A18})$$

Replacing the spherical Bessel functions by those of the first kind, one gets

$$\frac{\rho v_l^2}{R} [\xi j_0(\xi) - 4n^2 j_1(\xi)] = 0, \quad (\text{A19})$$

with  $\xi = hR = (\omega/v_l)R$  and  $n = v_t/v_l$ .

For a sphere embedded in a matrix, the stress vector no longer vanishes at the surface and has the same value approaching the surface from the inner and the outer radial directions. The same condition holds for the displacement vectors. Thus the general eigenvalue equation becomes

$$\det \left( \begin{pmatrix} D_{1r} & D_{2r} \\ D_{1n} & D_{2n} \\ S_{1r} & S_{2r} \\ S_{1n} & S_{2n} \end{pmatrix}_s \begin{pmatrix} D_{1r} & D_{2r} \\ D_{1n} & D_{2n} \\ S_{1r} & S_{2r} \\ S_{1n} & S_{2n} \end{pmatrix}_m \right) \Big|_{r=R} = 0, \quad (\text{A20})$$

with the material parameters of the sphere (with index  $s$ ) in the left two columns and those of the matrix (with index  $m$ ) in the right two columns. The Bessel functions within the sphere must be chosen as the  $j_l$  functions of the first kind and within the matrix as Hankel's functions  $h_l$ , which fades out into the matrix (outgoing waves).

In the case of  $l=0$ , the remaining displacement and stress vector components are  $D_{1r}$  and  $S_{1r}$  and, hence, the eigenvalue equation takes the simple form

$$\det \left[ \begin{pmatrix} D_{1r} \\ S_{1r} \end{pmatrix}_s \begin{pmatrix} D_{1r} \\ S_{1r} \end{pmatrix}_m \right]_{r=R} = 0. \quad (\text{A21})$$

In this case, with  $D_{1r} = z'_0 = -z_1$ , the eigenvalue equation can be transformed to

$$\frac{\rho_s v_{sl}^2}{R} [\xi_s j_0(\xi_s) - 4n_s^2 j_1(\xi_s)] / j_1(\xi_s) = \frac{\rho_m v_{ml}^2}{R} [\xi_m h_0(\xi_m) - 4n_m^2 h_1(\xi_m)] / h_1(\xi_m). \quad (\text{A22})$$

Replacing  $h_0(\xi_m)/h_1(\xi_m)$  by  $\xi_m/i\xi_m - 1$  we get

$$\xi_s j_0(\xi_s) - 4n_s^2 j_1(\xi_s) = \frac{\rho_m v_{ml}^2}{\rho_s v_{sl}^2} \left[ \frac{\xi_m^2}{i\xi_m - 1} - 4n_m^2 \right] j_1(\xi_s), \quad (\text{A23})$$

which can be rewritten into the eigenvalue equation (1) with  $n$  replaced by  $n_{\text{eff}}$  as given by Eq. (5).

- 
- <sup>1</sup>T. Itoh, Y. Iwabuchi, and M. Kataoka, *Phys. Status Solidi B* **145**, 567 (1988).  
<sup>2</sup>T. Itoh, Y. Iwabuchi, and M. Kataoka, *Phys. Status Solidi B* **146**, 531 (1988).  
<sup>3</sup>A. Nakamura, H. Yamada, and T. Tokizaki, *Phys. Rev. B* **40**, 8585 (1989).  
<sup>4</sup>A. I. Ekimov, Al. L. Efros, and A. A. Onushenko, *Solid State Commun.* **56**, 921 (1985).  
<sup>5</sup>T. Arai, H. Fujimura, I. Umeju, T. Ogawa, and A. Fujii, *Jpn. J. Appl. Phys., Part 1* **28**, 484 (1989).  
<sup>6</sup>N. F. Borrelli, D. W. Hall, H. J. Holland, and D. W. Smith, *J. Appl. Phys.* **61**, 5399 (1987).  
<sup>7</sup>S. Hayashi, M. Fujii, and K. Yamamoto, *Jpn. J. Appl. Phys., Part 2* **28**, L1464 (1989).  
<sup>8</sup>T. Bischof, M. Ivanda, G. Lermann, A. Materny, and W. Kiefer, *J. Raman Spectrosc.* **27**, 297 (1996).  
<sup>9</sup>M. Montagna and R. Dusi, *Phys. Rev. B* **52**, 10 080 (1995).  
<sup>10</sup>A. Tanaka, S. Onari, and T. Arai, *Phys. Rev. B* **47**, 1237 (1993).  
<sup>11</sup>A. Roy and A. K. Sood, *Solid State Commun.* **97**, 97 (1996).  
<sup>12</sup>L. Saviot, B. Champagnon, E. Duval, and A. I. Ekimov, *Phys. Rev. B* **57**, 341 (1998).  
<sup>13</sup>M. Rajalakshmi, T. Sakuntala, and A. K. Arora, *J. Phys.: Condens. Matter* **9**, 9745 (1997).  
<sup>14</sup>H. B. Abel, *Phys. Status Solidi B* **161**, 435 (1990).  
<sup>15</sup>A. Boukenter, B. Champagnon, E. Duval, J. L. Rousset, J. Dumas, and J. Serughetti, *J. Phys. C* **21**, L1097 (1988).  
<sup>16</sup>V. K. Malinovsky, V. N. Novikov, A. P. Sokolov, and V. C. Dodonov, *Solid State Commun.* **67**, 725 (1988).  
<sup>17</sup>B. Champagnon, B. Andrianasolo, and E. Duval, *J. Chem. Phys.* **94**, 5237 (1991).  
<sup>18</sup>J. A. Capobianco, P. P. Proulx, B. Andrianasolo, and B. Champagnon, *Phys. Rev. B* **43**, 10 031 (1991).  
<sup>19</sup>M. Fujii, T. Nagareda, S. Hayashi, and K. Yamamoto, *Phys. Rev. B* **44**, 6243 (1991).  
<sup>20</sup>H. Lamb, *Proc. London Math. Soc.* **13**, 189 (1882).  
<sup>21</sup>E. Duval, *Phys. Rev. B* **46**, 5795 (1992).  
<sup>22</sup>M. P. Chamberlain, C. Trallero-Giner, and M. Cardona, *Phys. Rev. B* **51**, 1680 (1995).  
<sup>23</sup>A. Tamura, K. Higata, and T. Ichinokawa, *J. Phys. C* **15**, 4975 (1982).  
<sup>24</sup>P. Verma, G. Irmer, J. Monecke and G. Goerigk (unpublished).  
<sup>25</sup>P. Verma, G. Irmer, and J. Monecke (unpublished).  
<sup>26</sup>E. Roca, C. Trallero-Giner, and M. Cardona, *Phys. Rev. B* **49**, 13 704 (1994).  
<sup>27</sup>A. Tanaka, S. Onari, and T. Arai, *Phys. Rev. B* **45**, 6587 (1992).  
<sup>28</sup>V. K. Malinovsky and A. P. Sokolov, *Solid State Commun.* **57**, 757 (1986).  
<sup>29</sup>A. P. Sokolov, A. Kistiuk, D. Quitmann, and E. Duval, *Phys. Rev. B* **48**, 7692 (1993).